Automatic Alignment of Fractured Femur: Integration of Robot and Optical Tracking System

Marzieh S. Saeedi-Hosseiny, Fayez Alruwaili, Michael P. Clancy, Emily A. Corson, Sean McMillan, Charalampos Papachristou, Nidhal C. Bouaynaya, *Member, IEEE*, Iulian I. Iordachita, *Senior Member, IEEE*, and Mohammad H. Abedin-Nasab

***Abstract*—This letter presents Robossis, a surgical robotic system for automated femur fracture alignment. Robossis is the integration of an optical tracking system with a 6-degree-of-freedom (6-DOF) 3-armed parallel robot that satisfies the clinical and mechanical design requirements for femur alignment surgery. In real-time, the optical tracking system obtains the spatial position of the distal and proximal parts of the fractured femur. Then, an auto-alignment algorithm uses this data to guide the robot to automatically and accurately align the bone fragments while overcoming the muscle payload surrounding the femur. A graphical user interface (GUI) provides a real-time visual guide for the surgeon to check the deviation from alignment while the robot is automatically bringing the bone into an aligned position. To demonstrate the capabilities of Robossis, laboratory and cadaver experiments are performed, showing that Robossis can successfully manipulate bone in 6 DOFs in space, achieving alignment with submillimeter accuracy.**

***Index Terms*—Robotic surgery, long-bone fractures, automatic alignment, fracture alignment, optical tracking, cadaver testing.**

I. Introduction

ANNUALLY, approximately 430000 femur fractures occur in the United States [1], [2], [3]. This incidence has increased in the past, and due to the aging population, it will likely increase in the future [1], [4]. Furthermore, the one-year mortality rate for femur fractures is 20-25% for the elderly [5], [6]. Despite the increasing occurrence of femoral fractures, femur fracture surgery results in rotational malalignment in more than a quarter of cases [7], [8]. These malalignments can be attributed to the manual alignment methods, the common femoral malrotation detection techniques, and the dependence on the skill of the surgeons [9], [10].

A misaligned femur can result in frontal plane malalignment, frontal plane knee joint misorientation, and a posterior shift of the weight-bearing axis in the sagittal plane [11], [12]. These issues are felt by the patient through pain in the hip and knee, limitations in movement, and the possibility of degenerative arthritis occurring [8].

In addition to the potential problems for the patient, there are negative effects on the hospital and medical staff carrying out these procedures, as malalignment requires reoperation in 17% of proximal femur fractures. Repeated surgeries introduce additional complications and costs and add to the healing time [13], [14], [15]. Moreover, this is a physically taxing operation for the surgical staff because they must counteract the surrounding muscles of the femur. The muscular forces limit the available range of motion in the operating area and often lead to damage of the surrounding soft tissue [16], [17], [18], [19]. To counteract these problems, multiple groups have attempted to introduce robots into femur surgeries.

Lee et al. [20] and Li et al. [21] attempted to improve upon the Stewart robotic platform. Lee et al. added a rotational ring frame to increase the mobility of the system. Experiments on femur phantoms and caprine legs were conducted and produced errors in the millimeter range, however, the proposed system's accuracy was not tested on a cadaver. Meanwhile, Li et al. designed their Stewart platform-based robot to be leader/follower teleoperated. Its feasibility was tested and showed promising results; however, the tests were done with just a bone model, so the forces of the muscles were not considered.

Two of the most fully developed robotic systems come from Kim et al. [17] and Dagnino et al. [22]. Kim et al. proposed a 6-DOF serial-type positioning robot and a 1-DOF traction device combination to improve the current workflow during long-bone fracture alignment surgery. However, the use of two robots increases the complexity of the system and requires the creation of a human-robot-robot cooperative control (HRRCC) scheme. Dagnino et al. [22] created a system that enables the simultaneous correction of two bone fragments by using two

Manuscript received 27 September 2022; accepted 20 February 2023. Date of publication 1 March 2023; date of current version 16 March 2023. This letter was recommended for publication by Associate Editor J.-J. Cabibihan and Editor P. Valdastri upon evaluation of the reviewers' comments. This work was supported in part by the National Science Foundation (NSF) under Grants 2141099 and 2226489 and in part by the New Jersey Health Foundation (NJHF) under Grant PC 62-21. *(Corresponding author: Mohammad H. Abedin-Nasab.)*

Marzieh S. Saeedi-Hosseiny, Emily A. Corson, and Nidhal C. Bouaynaya are with the Electrical and Computer Engineering Department, Rowan University, Glassboro, NJ 08028 USA (e-mail: saeedi64@rowan.edu; corson12@students.rowan.edu; bouaynaya@rowan.edu).

Fayez Alruwaili, Michael P. Clancy, and Mohammad H. Abedin-Nasab are with the Biomedical Engineering Department, Rowan University, Glassboro, NJ 08028 USA (e-mail: alruwa16@rowan.edu; clancym1@rowan.edu; abedin@rowan.edu).

Sean McMillan is with the Rowan University School of Osteopathic Medicine, Stratford, NJ 08084 USA, and also with the Virtua Health System, Willingboro, NJ 08046 USA (e-mail: smcmillan@virtua.org).

Charalampos Papachristou is with the Mathematics Department, Rowan University, Glassboro, NJ 0828 USA (e-mail: papachristou@rowan.edu).

Iulian I. Iordachita is with the Laboratory for Computational Sensing and Robotics, Johns Hopkins University, Baltimore, MD 21218 USA (e-mail: iordachita@jhu.edu).

This letter has supplementary downloadable material available at https://doi.org/10.1109/LRA.2023.3251198, provided by the authors.

Digital Object Identifier 10.1109/LRA.2023.3251198

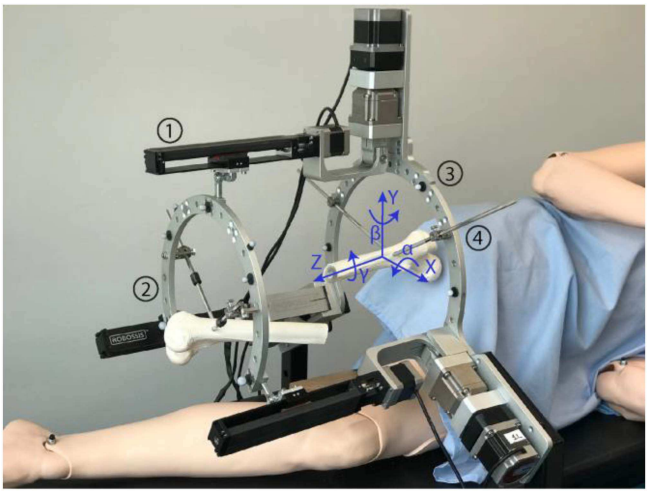

Fig. 1. Robossis, a surgical robot, during laboratory testing. The image depicts (1) the actuated arms, (2) the moving ring, (3) the fixed ring, and (4) the bone-gripping system, i.e., surgical Schanz screws. In this picture, the moving ring is in its home position: $X = Y = \alpha = \beta = \gamma = 0, Z = 275$ mm. The center of the workspace is considered to be the center of the moving ring, which is 275 mm from the fixed ring in the Z direction.

robotic fracture manipulators, each of which are 6-DOF parallel robots. Their design also includes an automated traction table, which is a 4-DOF device that pulls on the tibia to ensure proper alignment. However, of the nine cadavers tested, suboptimal alignments or worse were seen in four.

This letter describes the Robossis system, which integrates an optical tracking system with a unique robotic structure to implement an automatic alignment feature [23], [24], [25], [26]. The main contribution of this work is the alignment of the fractured femur with submillimeter accuracy using an automatic alignment algorithm, as demonstrated through multiple lab and cadaver tests. Robossis is the first surgical robot for femur fracture reduction surgery that utilizes an automatic alignment feature. This reduces the time spent in the operating room and the exposure to X-ray radiation. The remainder of this letter is organized as follows: Section II details the previous work done with Robossis, Section III outlines the navigation system, Section IV states the experiments and results, Section V provides a discussion of the work done, and Section VI is the conclusion.

II. Background

Robossis reached its current state after testing 6 different configurations. All of these underwent inverse kinematics, forward kinematics, and Jacobian analyses [23]. The wide-opened 3-armed mechanism was chosen for further development. Kinematic, Jacobian, dynamic, position-control, singularity, and workspace analyses were performed for this mechanism [24], [27], [28].

The current version of Robossis is a 6-DOF 3-RRPS parallel mechanism that consists of a fixed ring and a moving ring that are connected by three actuated arms (Fig. 1). Each arm consists of a universal (RR), prismatic (P), and spherical (S) joint, and it is capable of movement through rotary and linear actuators [29]. The rotary actuators are attached to the fixed ring and are connected to the linear actuators by universal joints. The linear actuators are attached to the moving ring by spherical joints [25]. The robot is connected to a rigid stand with locking wheels, which eliminates ground vibrations.

Besides the robot, there are three other systems a part of Robossis. The first system is a control panel that is run through MATLAB. This allows the surgeon to move the robot's moving ring, return the robot to its home position (Fig. 1), and enable an emergency stop. The second system is the leader controller that controls the movements of the robot through the Novint Falcon 3D Haptic Controller. This controller utilizes three different MATLAB codes: gravity, cylinder, and viscosity. The gravity code enables the last position to be maintained, the cylinder code keeps the movements of the controller within the workspace of the robot, and the viscosity code prevents sudden movements from affecting the overall position. The third system is the bone gripping system, which includes self-tapping half-pin surgical rods, that are attached to the fixed and moving rings of the robot via angled pin connectors [29].

III. Navigation System

The navigation system consists of two MATLAB GUIs, the Motive software, three OptiTrack Flex-13 cameras, and two uniquely designed rigid bodies (Fig. 2). On the rigid bodies, there are four motion capture markers that are tracked by the cameras. The custom rigid bodies are designed so that their center of geometry is at the junction of their four arms, where the Motive software reads the position of the rigid bodies (Fig. 2(7)). Motive, an optical motion capture software, was used to stream motion tracking data to Simulink where an S-Function block captures the data from Motive using NatNet SDK. Once the data is processed by Simulink, it is sent to a Speedgoat real-time target machine which allows the system to perform in real time.

A. Integration of Robot and Optical Tracking System

To match the position of the moving ring with the optical tracking system, five coordinate systems in the space were defined. Using this method, the necessary command can be given to the robot to move toward the final aligned position by only having the position data of two rigid bodies connected to the proximal and distal femur. The five required coordinate systems are defined on 1) the ground plane of the optical tracking system {OT}, 2) the center of the fixed ring {FR}, 3) the center of the moving ring {MR}, 4) the distal rigid body {DS}, and 5) the proximal rigid body {PX} (Fig. 3).

The optical tracking system gives us access to the 3D position of {DS} and {PX} in {OT} in real time. At the current stage of our development, to obtain the final relative position of the distal and proximal rigid bodies in the alignment position, the bone needs to be aligned and the position data of the markers using the optical tracking system needs to be recorded. Then, the transformation matrix of distal vs. proximal rigid bodies at alignment, ${}^{PX}T^{F}_{DS}$, was calculated using the streamed position

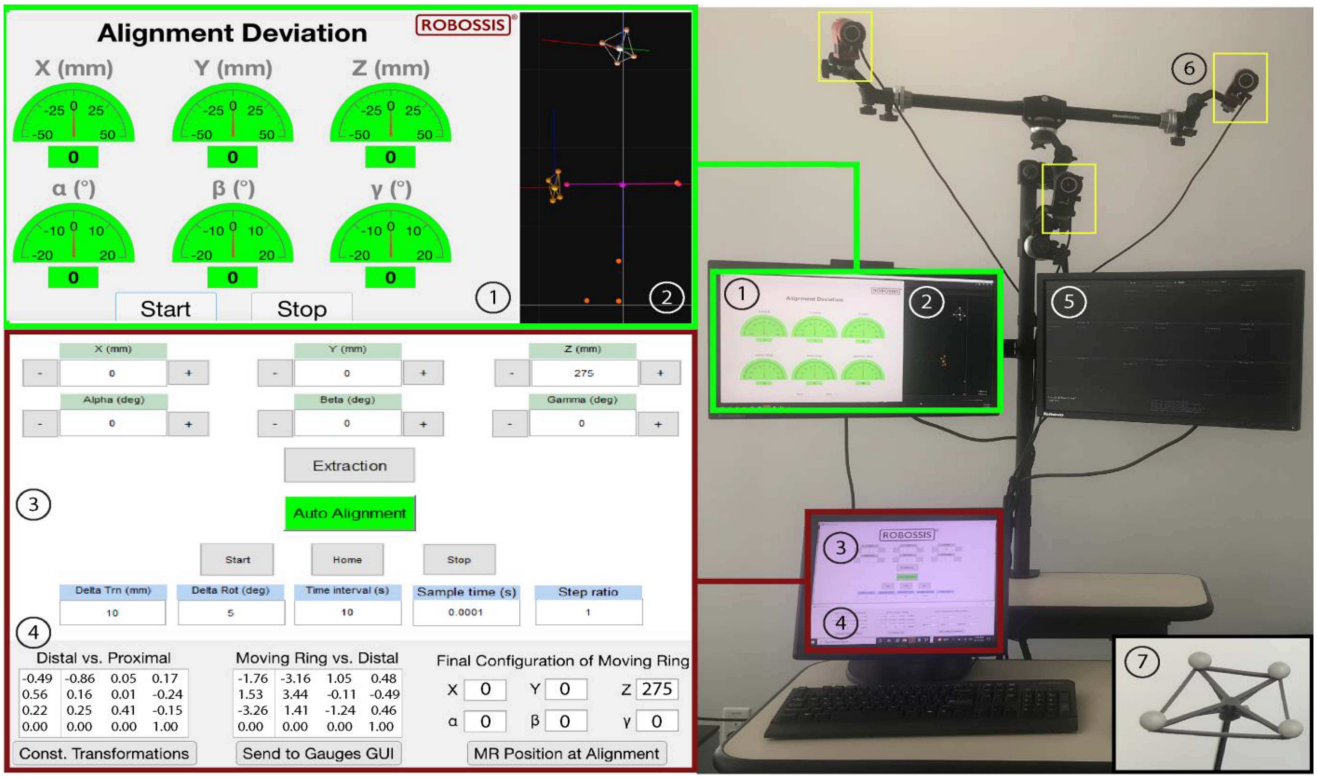

Fig. 2. Robossis workstation. (1) Gauges GUI displaying deviation from correct alignment in 6 DOFs in real time. The position data of the markers attached to the distal and proximal femur stream to the GUI from (2) Motive optical tracking software. (3) The control panel, which allows the surgeon to automatically align the bone, extract the bone segments apart from each other, or manipulate the distal femur in 6 DOFs, independently. (4) Imaging software GUI, a panel to set up the required data for the auto-alignment feature. (5) Speedgoat GUI, which illustrates the input signals to the robot's motors. (6) 3 OptiTrack Flex-13 cameras with 1.3 million pixels of resolution and a 56° field of view. (7) Rigid body designed to hold 4 motion capture markers.

data of the two rigid bodies from the Motive software to MATLAB and Simulink. To do so, the {PX} and {DS} coordinates were defined as follows:

$$\begin{aligned}
\{PX\}:\ \mathrm{Op} &= \begin{bmatrix} x_o^p \\ y_o^p \\ z_o^p \end{bmatrix},\ \bar{x}_p = \begin{bmatrix} x_1^p \\ y_1^p \\ z_1^p \end{bmatrix}, \\
\bar{y}_p &= \begin{bmatrix} x_2^p \\ y_2^p \\ z_2^p \end{bmatrix},\ \bar{z}_p = \begin{bmatrix} x_3^p \\ y_3^p \\ z_3^p \end{bmatrix} \qquad (1) \\
\{DS\}:\ \mathrm{Od} &= \begin{bmatrix} x_o^d \\ y_o^d \\ z_o^d \end{bmatrix},\ \bar{x}_d = \begin{bmatrix} x_1^d \\ y_1^d \\ z_1^d \end{bmatrix}, \\
\bar{y}_d &= \begin{bmatrix} x_2^d \\ y_2^d \\ z_2^d \end{bmatrix},\ \bar{z}_d = \begin{bmatrix} x_3^d \\ y_3^d \\ z_3^d \end{bmatrix} \qquad (2)
\end{aligned}$$

$\mathrm{O_p}$ and $\mathrm{O_d}$ are the origins of the {PX} and {DS}, respectively. These origins of the rigid bodies' coordinates are set to be in the center of their geometry, which are obtained from the Motive software directly. The markers' position and the geometric specifications of our designed rigid bodies are used to define the axes of {PX} and {DS}, which are $\bar{x}_p,\ \bar{y}_p,\ \bar{z}_p$ and $\bar{x}_d,\ \bar{y}_d,\ \bar{z}_d$, respectively.

$$^{OT}T_{PX} = \begin{bmatrix} \begin{bmatrix} x_1^p & x_2^p & x_3^p \\ y_1^p & y_2^p & y_3^p \\ z_1^p & z_2^p & z_3^p \end{bmatrix} & \begin{bmatrix} x_o^p \\ y_o^p \\ z_o^p \end{bmatrix} \\ \begin{bmatrix} 0 & 0 & 0 \end{bmatrix} & 1 \end{bmatrix} \qquad (3)$$

$$^{OT}T_{DS} = \begin{bmatrix} \begin{bmatrix} x_1^d & x_2^d & x_3^d \\ y_1^d & y_2^d & y_3^d \\ z_1^d & z_2^d & z_3^d \end{bmatrix} & \begin{bmatrix} x_o^d \\ y_o^d \\ z_o^d \end{bmatrix} \\ \begin{bmatrix} 0 & 0 & 0 \end{bmatrix} & 1 \end{bmatrix} \qquad (4)$$

Using the matrices (3) and (4), $^{PX}T_{DS}^{F}$ is calculated by the formula (5).

$$^{PX}T_{DS}^{F} = \left(^{OT}T_{PX}\right)^{-1}\left(^{OT}T_{DS}\right), \qquad (5)$$

which gives us the desired final relative position of the bone segments at alignment.

The other required transformation matrix is the transformation between the moving ring and the fixed ring ($^{FR}T_{MR}$), which is needed by the robot control system to guide the robot in moving from the initial fractured position to the final alignment position. This is needed since the control system considers the position of the moving ring (end-effector) relative to the fixed ring. In this step, the robot's moving ring is considered to be in its home position (X = Y = $\propto = \beta = \gamma = 0$, Z = 275 mm) and then

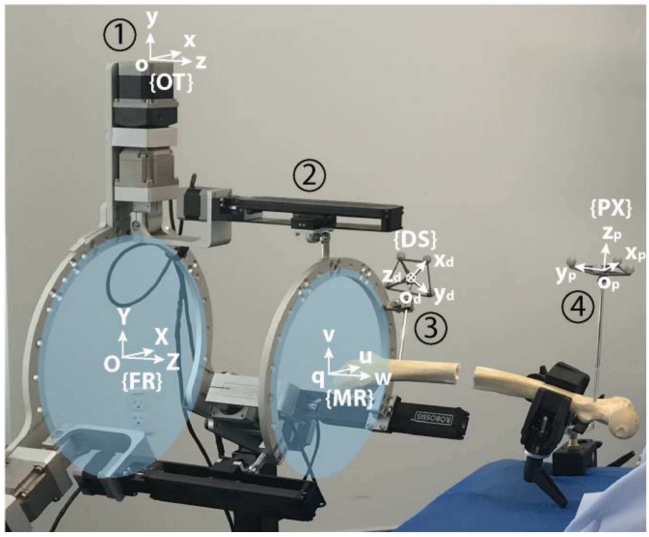

Fig. 3. Illustration of the five required coordinate systems for integration of robot and optical tracking system. The coordinates are {OT}: OptiTrack, {FR}: Fixed Ring, {MR}: Moving Ring, {DS}: Distal Rigid Body, and {PX}: Proximal Rigid Body. The picture shows (1) considered location for the OptiTrack ground plane, (2) middle arm of the robot, (3) distal rigid body connected to distal femur, and (4) proximal rigid body connected to proximal femur.

form the ${}^{FR}T_{MR}$:

$$ {}^{FR}T_{MR} = [1,0,0,0;0,1,0,0;0,0,1,275;0,0,0,1] \tag{6}$$

The next step is to compute the transformation matrix of the distal rigid body to the moving ring, ${}^{MR}T^{C}_{DS}$. This matrix is constant due to the fixed position of the {DS} relative to the {MR} during the operation. Using the matrix (6), ${}^{MR}T^{C}_{DS}$ is calculated by the formula (7):

$$ {}^{MR}T^{C}_{DS} = \left({}^{FR}T_{MR}\right)^{-1}\left({}^{FR}T^{C}_{OT}\right)\left({}^{OT}T_{DS}\right) \tag{7}$$

where ${}^{FR}T^{C}_{OT}$ can be calculated utilizing the relative position of the {OT} to the {FR}, which is fixed and known in our system design (see matrix (8)). The ground plane of the optical tracker is located on top of the motor of the robot's middle arm (Fig. 3(1)) and has only a translation of 39.2 mm in the Y-direction compared to the center of the fixed ring (Fig. 3).

$$ {}^{FR}T^{C}_{OT} = [1,0,0,0;0,1,0,39.2;0,0,1,0;0,0,0,1] \tag{8}$$

Now, the required constant transformation matrices, ${}^{PX}T^{F}_{DS}$ and ${}^{MR}T^{C}_{DS}$, have been obtained.

Then, using the control panel, the bone segments are moved to the fractured position to create an arbitrary fracture. The creation of the arbitrary fracture is only done during laboratory testing. In a real clinical procedure, the transformation matrices are obtained based on the desired patient bone anatomy.

Next, the final transformation matrix {DS} in {OT} is calculated. This matrix is needed to obtain the final 3D position of the moving ring so that the robot control system can guide the moving ring to reach the aligned position.

$$ {}^{OT}T^{F}_{DS} = \left({}^{OT}T_{PX}\right)\left({}^{PX}T^{F}_{DS}\right) \tag{9}$$

This gives us the final desired transformation matrix for {DS} in {OT}, independent of the proximal position in real time. The final transformation matrix of {MR} in {FR}, which gives us the required translations and rotations of the moving ring to achieve the desired alignment, can be achieved by the (10) and leads to the automatic alignment of the fracture.

$$ {}^{FR}T^{F}_{MR} = \left({}^{FR}T^{C}_{OT}\right)\left({}^{OT}T^{F}_{DS}\right)\left({}^{MR}T^{C}_{DS}\right)^{-1} \tag{10}$$

While the robot is automatically aligning the bone segments, the real-time position of {PX} and {DS} is captured to calculate the transformation matrix between the desired target position for the moving ring and the real-time position of the moving ring while aligning the bone. Therefore, the deviation from the alignment can be calculated when the robot operation is finished to check whether the desired alignment has been reached. To do so, ${}^{PX}T_{DS}$ is calculated in real-time using the formula (11).

$$ {}^{PX}T_{DS} = \left({}^{OT}T_{PX}\right)^{-1}.{}^{OT}T_{DS} \tag{11}$$

$$ {}^{DS^F}T_{DS} = \left({}^{PX}T^{F}_{DS}\right)^{-1}.{}^{PX}T_{DS} \tag{12}$$

${}^{DS^F}T_{DS}$ shows us the translation and rotation of the achieved {DS} position versus the desired one. To compare the achieved and desired position for the moving ring, ${}^{MR^F}T_{MR}$ is computed through the (13) and (14).

$$ {}^{DS^F}T_{MR} = {}^{DS^F}T_{DS}.\left({}^{MR}T^{c}_{DS}\right)^{-1} \tag{13}$$

$$ {}^{MR^F}T_{MR} = \left({}^{DS}T^{c}_{MR}\right)^{-1}.{}^{DS^F}T_{MR} = \begin{bmatrix} R_{11} & R_{12} & R_{13} & e_x \\ R_{21} & R_{22} & R_{23} & e_y \\ R_{31} & R_{32} & R_{33} & e_z \\ 0 & 0 & 0 & 1 \end{bmatrix} \tag{14}$$

Now, the translational and rotational deviations from alignment have been obtained, which are shown on the gauges GUI (Fig. 2(1)) during the robot's operation. The translation errors are determined using the (15), and the rotm2eul MATLAB function is used to find the XYZ Euler angles to find rotational errors as seen in (16).

$$ (x,y,z)_{dev} = \begin{bmatrix} e_x & e_y & e_z \end{bmatrix} \tag{15}$$

$$ (\alpha,\beta,\gamma)_{dev} = rotm2eul\left({}^{MR^F}R_{MR},'XYZ'\right) * 180/\pi \tag{16}$$

B. Clinical Workflow

The integration of Robossis into femur fracture alignment surgery introduces a novel clinical workflow, which is detailed in Fig. 4. Before surgery begins, the patient and Robossis are properly positioned. The patient is placed in the supine position. The moving ring of Robossis is then positioned to the distal fragment of the femur and Schanz screws are drilled into the proper positions on the distal and proximal bone fragments. The surgeons need to identify safe regions to insert the nails to ensure the patients' nerves are not at risk. The maximum speed of the robot is less than 2 mm/s to prevent any damage to the nerves. The distal screw gets connected to the moving ring of the robot.

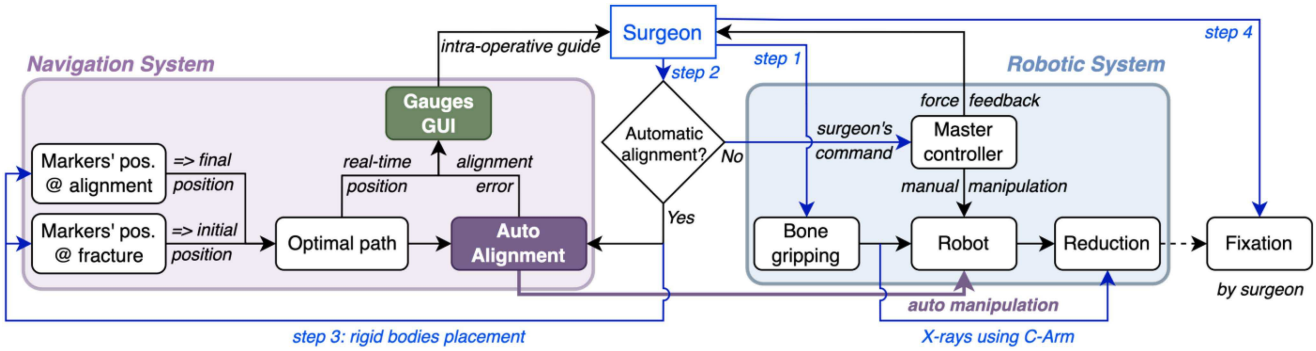

Fig. 4. The clinical workflow of the Robossis for femur fracture alignment surgery. The workflow is split into two parts: a navigation system and a robotic system. If the surgeon wants to use the auto-alignment feature, the navigation system is used to obtain the optimal alignment path. This information is then sent to the robotic system, and submillimeter alignment is reached. Using the navigation system also allows for the gauges GUI to provide a visual aid to the surgeon to show deviation from the alignment intra-operatively. If the surgeon wishes to manually align the fracture, the leader controller is used.

If the surgeon decides to use the navigation system, the rigid bodies are attached on top of the screws and the imaging software GUI is run, which obtains the required constant transformation matrices ${}^{PX}T^{F}_{DS}$ and ${}^{MR}T^{C}_{DS}$. This information is used to find the final configuration of the moving ring when the bone segments are aligned. Using the control panel, extraction is performed, which moves the bone fragments 10 mm apart in the Z-direction so that a collision does not occur during automatic alignment. The automatic alignment feature is then executed, and the robot automatically aligns the distal bone segment to the proximal segment. Anteroposterior (AP) and lateral X-ray images are taken with the C-arm before and after alignment. If the surgeon is satisfied with the X-ray images after alignment, then the alignment process is complete and bone fixation occurs by the surgeon. If the surgeon is not satisfied, adjustments can be made with the control panel until the desired aligned is achieved.

The addition of the Robossis system to the clinical workflow does present some limitations. It removes space from the surgeon's workspace and takes away their tactile sense of the patient's leg. The surgeons would also need to go through training to use the robot properly.

IV. Experiments and Results

To test the accuracy of the auto-alignment feature, laboratory and cadaver testing was conducted. Both tests followed a similar set-up procedure as detailed here. The steps unique to each test are outlined below in their respective sub-sections. The set-up procedure is as follows: 1) attach the Schanz screws to the bone segments, 2) attach the distal screw to the moving ring, 3) connect the rigid bodies onto the screws, 4) open the Motive software and calibrate the system, 5) run the imaging software GUI, 6) run the gauges GUI, and 7) turn on the robot and run the control panel.

A. Laboratory Testing

In addition to the set-up procedure detailed above, the two bone segments must be manually aligned and the proximal portion must be attached to a stationary object to run the trials.

TABLE I
Summary of the Ten Tests Conducted

X	Y	Z	α	β	γ	X-E	Y-E	Z-E
-20	0	0	0	0	0	0.07	0.01	0.02
0	-20	0	0	0	0	-0.01	0.06	0.02
0	0	-20	0	0	0	-0.01	0.03	0.01
-20	-20	-20	0	0	0	0.03	0.07	0.06
-40	-40	-40	0	0	0	0.01	-0.05	0.06
0	0	0	+5	0	0	0.00	0.02	-0.03
0	0	0	0	+5	0	-0.05	-0.06	-0.01
0	0	0	0	0	+5	0.02	0.03	0.01
0	0	0	+5	+5	+5	0.00	0.00	-0.02
-40	-40	-40	+5	+5	+5	-0.1	-0.07	-0.01

The X, Y, Z, ALPHA, BETHA, and GAMMA values represent the amount of movement of the robot in that direction for each test in millimeters or degrees. The last three columns show the median errors in the X, Y and Z directions in mm.

To test the accuracy of the robot's movement while performing auto-alignment, ten sets of tests were conducted, and they were divided into five translational paths, four rotational paths, and one combined movement path. The five translational tests were -20 mm in the X-direction; -20 mm in the Y-direction; -20 mm in the Z-direction; -20 mm in all the X-, Y-, and Z-directions; and -40 mm in the X-, Y-, and Z-directions. The four rotational tests were $+5°$ in the α-rotation; $+5°$ in the β-rotation; $+5°$ in the γ-rotation; and $+5°$ in the α-, β-, and γ-rotations. The combined movement test was -40 mm in the X-, Y-, and Z-directions and $+5°$ in the α-, β-, and γ-rotations. These tests can be seen in Table I along with their resulting median errors in the X, Y, and Z-directions in mm.

Each test had eight trials. For each trial, the initial X, Y, and Z position of the moving ring was recorded, the control panel was used to move the moving ring to the fracture position, the auto-alignment feature was applied, and then the final X, Y, and Z position of the moving ring was recorded. The deviations shown on the gauges GUI were also recorded at the initial and final positions.

After completing all the tests, the deviations between the initial and final positions in the X-, Y-, and Z- directions were

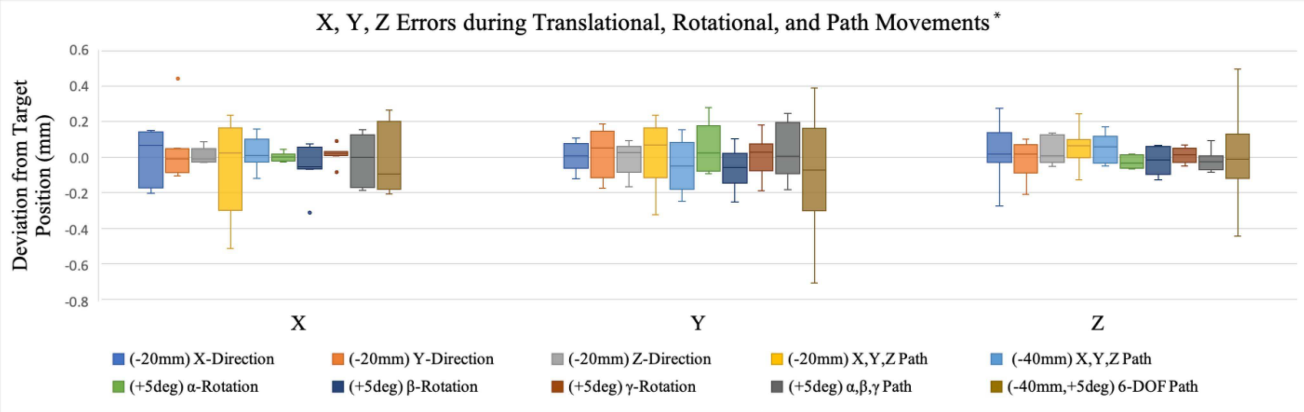

Fig. 5. Test results of translational, rotational, and path movements. The median errors from each of the ten different movements in the X-, Y-, and Z-directions are always a value between −0.2 mm and 0.2 mm. These results exceed the clinical requirements for femur fracture alignment surgery.
*None significantly different from zero (all p-values > 0.05).

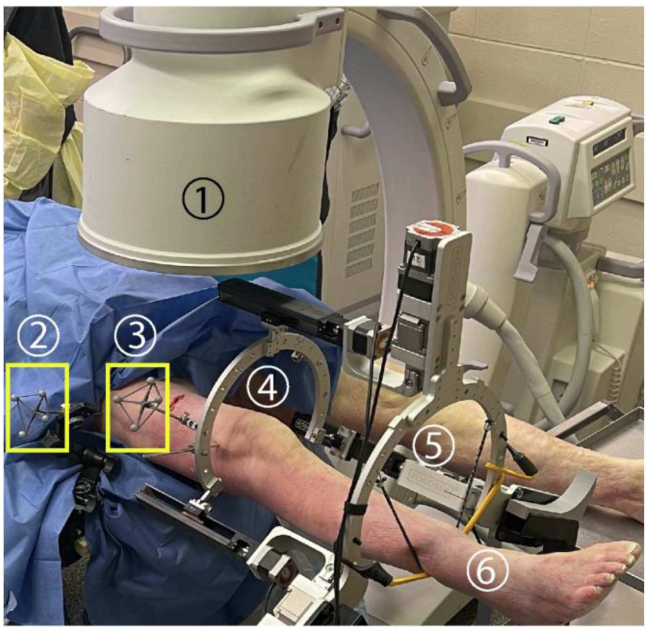

Fig. 6. Robossis in use during cadaver testing to simulate a real-life surgery. The cadaver allows Robossis to be tested against the muscle forces around the femur. To conduct the surgery, extraction is done followed by use of the robot's automatic alignment feature. When the automatic alignment is complete, the fracture position can be checked by taking AP and lateral X-ray images. The surgical setup includes (1) C-arm, (2) markers on proximal fragment, (3) markers on distal fragment, (4) the moving ring, (5) the fixed ring, and (6) an 89-year-old male cadaver.

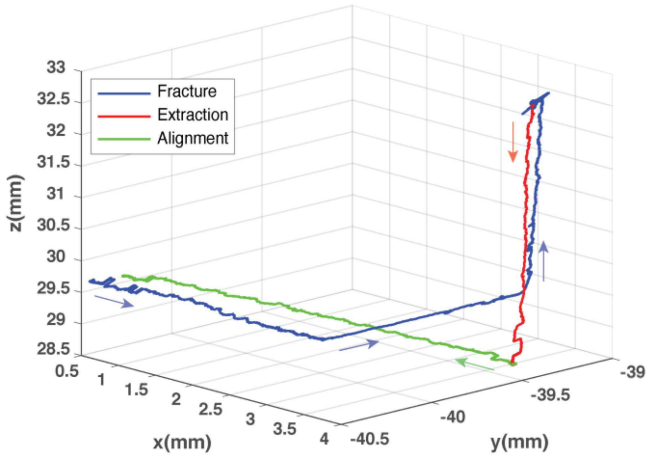

Fig. 7. Trajectory of the moving ring of Robossis during cadaver testing. To show the path that the moving ring of Robossis takes during the creation of the fracture (blue), extraction (red), and auto-alignment (green), a .tak file was captured from the Motive software. This file contained the X-, Y-, and Z-coordinates for the moving ring throughout the paths it took. The exact starting position was reached in the X- and Z-directions, while there is a slight error of 0.2 mm in the Y-direction.

calculated. The deviations for each direction are displayed in Fig. 5. The median deviations for each test are always a value between −0.2 mm and 0.2 mm. A majority of the median errors were extremely close to 0, indicating that, on average, the moving ring of the robot reached the correct position. All the absolute value maximum deviations were less than 0.7 mm.

When looking at Fig. 5 and comparing the errors present in the X-, Y-, and Z-directions, the errors in the Y-direction were the greatest. This is caused by the clearance issue for the joints of the robot's middle arm (Fig. 3(2)) and gravity, because the middle arm is vital in Y-direction movement (upward vertical movement). Since the direction of gravity is in the same direction as Y, there were slightly larger errors present in the Y direction. However, in all cases except for one, the absolute value of the errors in the Y-direction are all less than 0.5 mm.

The rotational errors were captured through the gauges GUI. For all the translational, rotational, and combined path laboratory testing, most of the rotational errors were 0°. In scenarios where it was not 0°, the errors were 1° or 2°, which is a much smaller rotation than the maximum acceptable rotation considered to be "Excellent Alignment" which is 5° [30]. Finally, for each condition and each of the three directions (X, Y, and Z), the obtained Wilcoxon signed rank test p-values for comparing the mean error to zero were all much greater than 0.05 under every condition tested, demonstrating the robot's ability to reach the exact desired position using the auto-alignment feature.

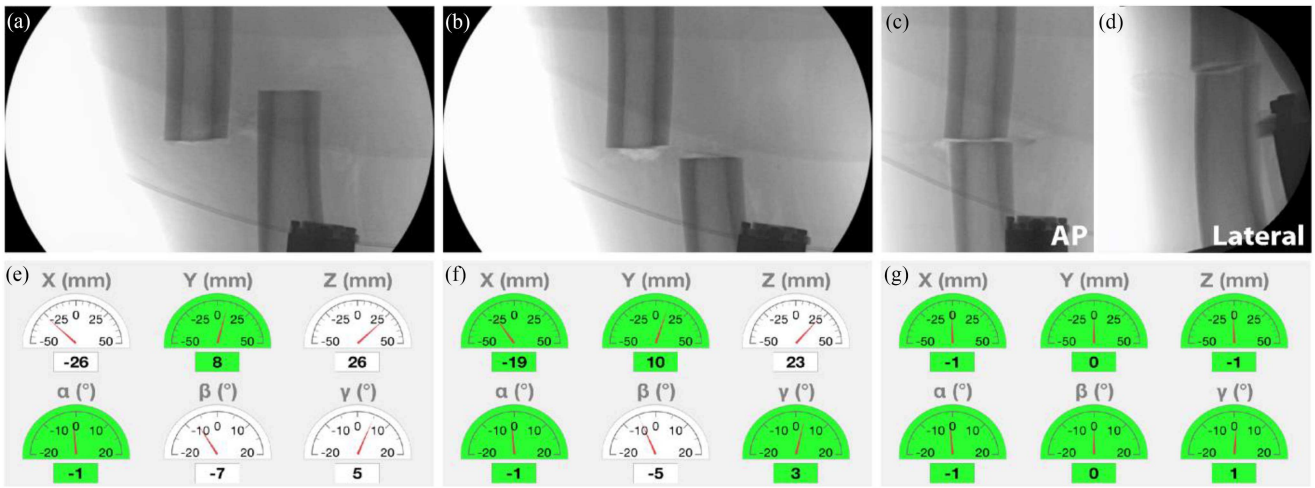

Fig. 8. X-ray images of (a) initial position of the fracture, (b) position of the femur fragments after extraction, (c) aligned femur using Auto-Alignment feature from AP and (d) lateral view, which show that the correct alignment was achieved. The gauges are showing deviation from alignment (e) at the initial position, (f) while performing auto-alignment, and (g) at the aligned position, where there is a maximum of 1 mm deviation from desired alignment.

B. Cadaver Testing

To perform the cadaver experiment, the cadaver must be placed in the supine position, the foot of the fractured leg must be hung from the fixed ring, the moving ring of the robot needs to be positioned to the distal fragment, and Schanz screws must be drilled into the distal and proximal bone fragments (Fig. 6). Furthermore, the femur of the cadaver is intact when brought to the operating room. Once the steps outlined in this section are performed, the femur is broken with a saw.

After breaking the bone, a fracture desired by the surgeon is created with the robot. The aligned position is taken after the femur is broken, but before the desired fracture is positioned. At this point, the set-up procedure from above is followed. After that, AP and lateral X-ray images are taken.

To align the bone, extraction was performed to move the bone segments apart in the Z-direction, and then auto-alignment was applied. The trajectory of the moving ring for the cadaver experiment can be seen in Fig. 7. This trajectory has near-zero errors in the X- and Z-directions but 0.2 mm error in the Y-direction. This can be explained by the previously mentioned problems involving the joint of the middle arm; therefore, this error is expected. The trajectory path has slight oscillations that are no more than 0.1 mm in each direction.

X-ray images and screenshots from the gauges GUI were taken throughout the procedure, as seen in Fig. 8. Alignment was achieved after the auto-alignment feature was used and all gauges showed minimal or no deviations from the desired aligned position gathered at the beginning of this test.

V. Discussion

For our auto-alignment feature to be applicable for femoral fracture alignment surgery, it must meet clinical requirements of approximately 1 cm and 5^{o} or less of translational and rotational deviation from the desired aligned position. This amount of translational and rotational deviation is rated as "Excellent Alignment" in the surgeon community [30].

For laboratory testing, under all the tested conditions, the maximum observed absolute error in any translational direction was less than 0.51 mm, except in one case when it was 0.7 mm. Furthermore, the rotational errors were usually zero or occasionally no more than 1° or 2°, which is less than half of the acceptable amount of error. For cadaver testing, as seen in Fig. 8, the gauges show 0 and 1 deviations from alignment in all DOFs. Considering the precision of the optical tracking system, which is 0.5 mm, the result of automatic alignment under muscle forces using the Robossis system is outstanding. The Robossis surgical robotic system demonstrated submillimeter accuracy, which exceeds clinical requirements, through laboratory and cadaver testing using its auto-alignment feature, clearly showcasing a superior ability to correctly align broken bones. This superior ability does not come at a manufacturing cost since the robot components have been designed with normal tolerances. This cadaver test also showed that a minimally invasive surgery can achieve optimal results. The only incisions that must be made are the two holes that are drilled for the Schanz screws and the hole for the intramedullary nail used for fixation.

After alignment is achieved, the surgeon needs to fix the bones in place. This is usually done by passing an intramedullary nail through the bone canal of the two bone fragments [10], [31], [32]. Nail fixation is easier to accomplish with the use of Robossis because once alignment is reached, the bone fragments are held in their exact alignment position. However, any fixation method could be used, not just nail fixation, because the surgeon is not limited by the possible movement of the bones while fixation occurs. During manual surgery, there is nothing holding the bone segments securely in place during the fixation process.

For cadaver testing, the desired final position for alignment was captured by the optical tracking system after cutting the femur but before creating the fracture. This method would not be feasible for real-life femur fracture alignment surgery, because the femur is already fractured when brought into the operating room. In future work, the X-ray images will be used to find the unbroken bone landmarks and the relative position of those

landmarks in the distal and proximal parts, which are the desired final positions for the fractured bone segments. Furthermore, manually identifying the required anatomical landmarks in the X-ray images would be time consuming; therefore, the plan is to implement machine learning models to automatically identify these landmarks. Additional future work will be focused on further optimizing the system by developing all the MATLAB and Simulink codes in C++.

VI. Conclusion

This letter presented a surgical robotic system for automatic alignment of femur fractures, called Robossis. Robossis consists of a newly developed navigation system coupled with a 3-armed 6-DOF parallel robot, which automatically aligns the femur fracture with submillimeter accuracy. The navigation system acquires the real-time positions of the rigid bodies attached to the distal and proximal parts of the femur, which are the inputs to the developed auto-alignment algorithm. The robot automatically aligns the distal femur to the proximal part by the auto-alignment feature, while the surgeon can keep track of the alignment process using the developed gauges GUI. The proposed automated system has significant advantages over manual methods currently used in the operating room, as it avoids reoperations, improves patient outcomes, and allows for less radiation exposure while providing an easier workflow for medical staff. Laboratory and cadaver experiments validate Robossis as a viable option for use in real surgical settings, as the robotic system can successfully achieve correct alignment with submillimeter accuracy, which exceeds the clinical requirements for femur fracture alignment surgeries.

References

[1] A. C. Ng et al., "Trends in subtrochanteric, diaphyseal, and distal femur fractures, 1984–2007," *Osteoporosis Int.*, vol. 23, no. 6, pp. 1721–1726, 2012.

[2] N. Enninghorst, D. McDougall, J. A. Evans, K. Sisak, and Z. J. Balogh, "Population-based epidemiology of femur shaft fractures," *J. Trauma Acute Care Surg.*, vol. 74, no. 6, pp. 1516–1520, 2013.

[3] C. L. Leibson, A. N. A. Tosteson, S. E. Gabriel, J. E. Ransom, and L. J. Melton III, "Mortality, disability, and nursing home use for persons with and without hip fracture: A population-based study," *J. Amer. Geriatrics Soc.*, vol. 50, no. 10, pp. 1644–1650, 2002.

[4] C. M. Court-Brown and B. Caesar, "Epidemiology of adult fractures: A review," *Injury*, vol. 37, no. 8, pp. 691–697, 2006.

[5] N. Lundin, T. T. Huttunen, A. Enocson, A. I. Marcano, L. Felländer-Tsai, and H. E. Berg, "Epidemiology and mortality of pelvic and femur fractures—A nationwide register study of 417,840 fractures in Sweden across 16 years: Diverging trends for potentially lethal fractures," *Acta Orthopaedica*, vol. 92, no. 3, pp. 323–328, 2021.

[6] O. Wolf, S. Mukka, J. Ekelund, M. Möller, and N. P. Hailer, "How deadly is a fracture distal to the hip in the elderly? An observational cohort study of 11,799 femoral fractures in the Swedish Fracture Register," *Acta Orthopaedica*, vol. 92, no. 1, pp. 40–46, 2020.

[7] R. L. Jaarsma, D. F. M. Pakvis, N. Verdonschot, J. Biert, and A. van Kampen, "Rotational malalignment after intramedullary nailing of femoral fractures," *J. Orthopaedic Trauma*, vol. 18, no. 7, pp. 403–409, 2004.

[8] R. L. Jaarsma and A. van Kampen, "Rotational malalignment after fractures of the femur," *J. Bone Joint Surg.*, vol. 86, no. 8, pp. 1100–1104, Nov. 2004.

[9] L. S. Marchand, L. G. Jacobson, A. R. Stuart, J. M. Haller, T. F. Higgins, and D. L. Rothberg, "Assessing femoral rotation: A survey comparison of techniques," *J. Orthopaedic Trauma*, vol. 34, no. 3, pp. e96–e101, Mar. 2020.

[10] L. Bai, J. Yang, X. Chen, Y. Sun, and X. Li, "Medical robotics in bone fracture reduction surgery: A review," *Sensors*, vol. 19, no. 16, Aug. 2019, Art. no. 3593.

[11] O. Kessler, S. Patil, C. W. Colwell Jr., and D. D. D'Lima, "The effect of femoral component malrotation on patellar biomechanics," *J. Biomech.*, vol. 41, no. 16, pp. 3332–3339, 2008.

[12] J. J. M. Gugenheim, R. A. M. Probe, and M. R. M. Brinker, "The effects of femoral shaft malrotation on lower extremity anatomy," *J. Orthopaedic Trauma*, vol. 18, pp. 658–664, 2004.

[13] J. T. Patterson et al., "Open reduction is associated with greater hazard of early reoperation after internal fixation of displaced femoral neck fractures in adults 18-65 years," *J. Orthopaedic Trauma*, vol. 34, no. 6, pp. 294–301, Jun. 2020.

[14] J. M. Drew, W. L. Griffin, S. M. Odum, B. van Doren, B. T. Weston, and L. S. Stryker, "Survivorship after periprosthetic femur fracture: Factors affecting outcome," *J. Arthroplasty*, vol. 31, no. 6, pp. 1283–1288, Jun. 2016.

[15] L. J. Lapidus, A. Charalampidis, J. Rundgren, and A. Enocson, "Internal fixation of garden I and II femoral neck fractures: Posterior tilt did not influence the reoperation rate in 382 consecutive hips followed for a minimum of 5 years," *J. Orthopaedic Trauma*, vol. 27, no. 7, pp. 386–390, Jul. 2013.

[16] G. Dagnino, I. Georgilas, P. Köhler, S. Morad, R. Atkins, and S. Dogramadzi, "Navigation system for robot-assisted intra-articular lower-limb fracture surgery," *Int. J. Comput. Assist. Radiol. Surg.*, vol. 11, no. 10, pp. 1831–1843, Oct. 2016.

[17] W. Y. Kim, S. Joung, H. Park, J.-O. Park, and S. Y. Ko, "Human-robot-robot cooperative control using positioning robot and 1-DOF traction device for robot-assisted fracture reduction system," *Proc. Inst. Mech. Engineers, Part H: J. Eng. Med.*, vol. 236, no. 5, pp. 697–710, May 2022.

[18] S. Zhu et al., "A marker-free 2D image-guided method for robot-assisted fracture reduction surgery," *J. Intell. Robot. Syst.*, vol. 103, no. 4, pp. 1–19, Nov. 2021.

[19] P. K. Jamwal, S. Hussain, and M. H. Ghayesh, "Intrinsically compliant parallel robot for fractured femur reduction: Mechanism optimization and control," *Robot. Auton. Syst.*, vol. 141, 2021, Art. no. 103787.

[20] S. Lee et al., "3D Image-guided robotic system for bone fracture reduction," *IEEE Robot. Automat. Lett.*, vol. 7, no. 2, pp. 4353–4360, Apr. 2022.

[21] C. Li et al., "A novel master-slave teleoperation robot system for diaphyseal fracture reduction: A preliminary study," *Comput. Assist. Surg.*, vol. 21, pp. 162–167, 2016.

[22] G. Dagnino et al., "Image-guided surgical robotic system for percutaneous reduction of joint fractures," *Ann. Biomed. Eng.*, vol. 45, no. 11, pp. 2648–2662, 2017.

[23] M. H. Abedinnasab, F. Farahmand, B. Tarvirdizadeh, H. Zohoor, and J. Gallardo-Alvarado, "Kinematic effects of number of legs in 6-DOF UPS parallel mechanisms," *Robotica*, vol. 35, no. 12, pp. 2257–2277, 2017.

[24] M. H. Abedin-Nasab and M. S. Saeedi-Hosseiny, "Robossis: Orthopedic surgical robot," in *Handbook of Robotic and Image-Guided Surgery*. Amsterdam, The Netherlands: Elsevier, 2020, pp. 515–528, doi: 10.1016/b978-0-12-814245-5.00030-x.

[25] F. Alruwaili, M. S. Saeedi-Hosseiny, L. Guzman, S. McMillan, I. I. Iordachita, and M. H. Abedin-Nasab, "A 3-armed 6-DOF parallel robot for femur fracture reduction: Trajectory and force testing∗," in *Proc. Int. Symp. Med. Robot.*, 2022, pp. 1–6.

[26] M. Abedin-Nasab, "Surgical robot," U.S. Patent 10,603,122 B2, Mar. 31, 2020.

[27] M. H. Abedinnasab, F. Farahmand, and J. Gallardo-Alvarado, "The wide-open three-legged parallel robot for long-bone fracture reduction," *J. Mechanisms Robot.*, vol. 9, no. 1, 2017, Art. no. 015001.

[28] M. H. Abedinnasab, J. G. Alvarado, B. Tarvirdizadeh, and F. Farahmand, "Sliding-mode tracking control of the 6-dof 3-legged wide-open parallel robot," in *Parallel Manipulators: Design, Applications and Dynamic Analysis*. Hauppauge, NY, USA: Nova Science Publishers, 2016, pp. 143–166.

[29] M. S. Saeedi-Hosseiny, F. Alruwaili, S. McMillan, and I. Iordachita, and M. H. Abedin-Nasab, "A surgical robotic system for long-bone fracture alignment: Prototyping and cadaver study," *IEEE Trans. Med. Robot. Bionics*, vol. 4, no. 1, pp. 172–182, Feb. 2022.

[30] C. K. Yu, V. A. Singh, S. Mariapan, and S. T. B. Chong, "Antegrade versus retrograde locked intramedullary nailing for femoral fractures: Which is better?," *Eur. J. Trauma Emerg. Surg.*, vol. 33, no. 2, pp. 135–140, 2007.

[31] I. Kempf, A. Grosse, and G. Beck, "Closed locked intramedullary nailing. Its application to comminuted fractures of the femur," *J. Bone Joint Surg.*, vol. 67, no. 5, pp. 709–720, Jun. 1985.

[32] G. W. W. Ii, "Intramedullary nailing of femoral and tibial shaft fractures," *J. Orthopaedic Sci.*, vol. 11, pp. 657–669, 2006.